J. Min. Metall. Sect. B-Metall., 56 (3) (2020) 307 - 319

Journal of Mining and Metallurgy, Section B: Metallurgy

INFLUENCE OF LANCE HEIGHT AND ANGLE ON THE PENETRATION DEPTH OF INCLINED COHERENT AND CONVENTIONAL SUPERSONIC JETS IN ELECTRIC ARC FURNACE STEELMAKING

X.-T. Wu [a,b], R. Zhu [a,b], G.-S. Wei [a,b*], K. Dong [a,b]

[*a] School of Metallurgical and Ecological Engineering, University of Science and Technology, Beijing, China
[b] Beijing Key Laboratory of Research Center of Special Melting and Preparation of High-end Metal Materials, University of Science and Technology, Beijing, China

(Received 25 February 2019; accepted 11 September 2020)

Abstract

Nowadays, coherent and conventional supersonic jets are widely used in electric arc furnace (EAF) steelmaking processes. Generally, these jets are installed in the EAF oven wall with a tilt angle of 35–45°. However, limited studies have been conducted on the impact characteristics of these inclined supersonic jets. This study developed an optimized theoretical model to calculate the penetration depth of inclined coherent and conventional supersonic jets by combining theoretical modeling and numerical simulations. The computational fluid dynamics results are validated against water model experiments. A variable k is newly defined to reflect the velocity variation, which is related to the jet exit at the jet free distance. The results of the optimized theoretical model show that the lance height and lance angle influence the penetration depth of the inclined supersonic jet. At the same lance angle, the penetration depth decreases with the increase in the lance height. Similarly, it decreases with the decrease in lance angle at the same lance height. In addition, the penetration depth of an inclined coherent supersonic jet is larger than that of an inclined conventional supersonic jet under the same conditions. An optimized theoretical model can accurately predict the penetration depths of the inclined coherent and conventional supersonic jets.

Keywords: *Penetration depth; Inclined jets; EAF steelmaking; Lance height; Lance angle*

1. Introduction

Coherent and conventional supersonic jets, which are the key to increasing the melting intensity to satisfy the requirements of fast rhythm, low cost, and high quality, have been widely used in the modern electric arc furnace (EAF) steelmaking processes [1-3]. In most EAFs worldwide, these two supersonic jets are installed in the oven wall with a tilt angle and the angle between the jet central axis and horizontal level is in the range 35° to 45°. These inclined supersonic jets play an important role in the steelmaking process because they control the chemical reaction, bath stirring, kinetics, foaming slag formation, energy consumption, bath recirculation, and the occurrence of splashing [4]. Typically, the penetration depth of the jet reflects the stirring efficiency of the oxygen jet on the molten bath to some degree. Generally, the penetration depth of a molten bath is controlled by adjusting the lance height, lance angle, and gas flow rate in industrial production [5].

It is difficult to measure the characteristic parameters of the impact cavity under actual process conditions. In the field of operation optimization of oxygen supply, the interaction of a gas-jet with a liquid surface has been described extensively in the literature. M. Li [6] et al. systematically studied the impact characteristics of multiple gas jets in a converter via theory and experiment, and subsequently developed a theoretical model to predict the cavity depth of a two-layer liquid bath impinged by multiple gas jets in BOF. They also analyzed the transfer characteristics of momentum and energy at the time of jetting of oxygen into the molten bath using the multi-fluid volume of a fluid model. Collins [7] conducted extensive experiments to investigate the effect of jet momentum, lance angle, and lance height (distance from lance exit to molten steel surface). Molloy [8] analyzed the oscillatory nature of the impinging jet system and proposed three different modes (dimpling, splashing, and penetrating) with

*Corresponding author: wgshsteel@126.com

https://doi.org/10.2298/JMMB190225019W

respect to the impact of the jet on the liquid surface. Bapin [9] studied the droplet generation characteristics in a top-blowing steelmaking converter and observed that the ambient furnace temperature influences the droplet generation by affecting the attenuation of jet velocity. Solórzano-López [10] used mathematical and physical simulations, and compared different formulas of the cavity depth to analyze the interaction between a gas jet and a liquid free surface. Nordquist [11] used a water model experiment to determine the effect of the lance height and nozzle diameters on the penetration depth. Mikael Ersson [12] built a fundamental mathematical model of a top-blown bath and studied the flow field and surface deformation caused by an impinging jet. Muñoz-Esparza [13] developed a three-dimensional numerical model, which can present the flapping motion of the jet and cavity oscillations. Sabah and Brooks [14] investigated the splash distribution in oxygen steelmaking by a cold model experiment and used the principle of energy balance to analyze the power of the air jet around gas injection. Li and Harris [15] studied gas dispersion phenomena and used a water model experiment and theoretical analysis to model the gas bubble volume of a narrow slot in a liquid. Alam [16] investigated the relationship between the critical penetration depth and the lance angle in EAF steelmaking processes using theoretical and water models. Lee [17] believed that the cavities formed by an inclined gas jet oscillated owing to the wave generated by the gas jet and the wave propagated along the base of the cavity. In addition, the fluid flow characteristics of a conventional supersonic jet were thoroughly studied and widely reported. Similar studies were conducted for the fluid flow characteristics of a coherent supersonic jet [18-20]. Recently, our research team has investigated the impact characteristics of coherent and conventional supersonic jets in the vertical direction, providing some useful insights into the supersonic oxygen supplement [21, 22]. However, the research results are not suitable for reflecting the impact characteristics of inclined supersonic jets. The lance angle has a significant influence on the penetration of the jet, molten bath stirring, and molten slag splashing. Moreover, compared with a vertical supersonic jet, it is difficult to model the penetration of inclined supersonic jet owing to the existence of tilt angle. Hence, scant research has focused on the effect of lance height and lance angle on the penetration depth of inclined coherent and conventional supersonic jets.

This issue has focused on analyzing the penetration depth of inclined coherent and conventional supersonic jets in EAF steelmaking processes. The validity of the computational fluid dynamics (CFD) model is first examined using hydraulic experiments. An optimized theoretical model is thereafter built to calculate the penetration depth of these two inclined supersonic jets by integrating the theoretical model and the CFD model. The optimized theoretical model results are anastomosed to the CFD model data. Moreover, the influences of lance height and lance angle on the penetration depth of these two inclined supersonic jets are analyzed.

2. Numerical Modeling and Hydraulic Experiment

2.1 Numerical Modeling

2.1.1 Assumptions

(1) The flows of liquid and oxygen were three-dimensional, transient, and non-isothermal.

(2) The gas phase was regarded as a compressible Newtonian fluid and the liquids were regarded as incompressible Newtonian fluids.

(3) A nonslip condition was applied to all the walls. A standard wall function was used to model the mean velocities close to the wall.

(4) The chemical reactions in the molten bath were not considered.

2.1.2 Governing Equations

For a cell of an n-phase system, the volume fraction of i-th phase is α_i, and the sum of volume fractions of each phase in a cell is 1.

$$\sum_{i=1}^{n}\alpha_i = 1 \tag{1}$$

The continuity, momentum, and energy conservation equations are, respectively, given by Eq. (2) -(4).

$$\frac{1}{\rho_i}\left[\frac{\partial}{\partial t}\left(\alpha_i\rho_i\right)+\nabla\cdot\left(\alpha_i\rho_i v_i\right)=S_{\alpha_i}+\sum_{i=1}^{n}\left(m_{ji}-m_{ij}\right)\right] \tag{2}$$

$$\frac{\partial}{\partial t}\left(\rho\vec{v}\right)+\nabla\cdot\left(\rho\vec{v}\vec{v}\right)=-\nabla p+\nabla\cdot\left[\mu\left(\nabla\vec{v}+\nabla\vec{v}^{\prime}\right)\right]+\rho\vec{g}+F \tag{3}$$

$$\frac{\partial(\rho E)}{\partial t}+\nabla\cdot\left(u(\rho E+p)\right)=\nabla\cdot\left(k_{eff}\nabla T\right)+S_h \tag{4}$$

where ρ and ρ_i are, respectively, the density of the gas and the i-th phase, $kg\cdot m^{-3}$; v is the instantaneous velocity of fluid, $m\cdot s^{-1}$; v_i is the velocity component in the direction i, $m\cdot s^{-1}$; m_{ij} is the mass flowing from the i-th phase to the j-th phase, kg; m_{ji} is the mass flowing from the j-th phase to the i-th phase, kg; t is the time, s; $S_{\alpha i}$ is the custom source. p is pressure, MPa; μ is the dynamic viscosity, Pa·s; g is the volume force of gravity, N; F is the volume force from other outside, N.

The energy *E* can be determined by the mass average method in the VOF model, which is

expressed as follows:

$$E = \frac{\sum_{i=1}^{n} \alpha_i \rho_i E_i}{\sum_{i}^{n} \alpha_i \rho_i} \quad (5)$$

where E_i for each phase is based on the specific heat of the phase and the shared temperature. The effective thermal conductivity, k_{eff}, and ρ_i are shared by the phases. The source term S_h contains contributions from radiation and any other volumetric heat sources [23].

The standard k–ε turbulence model was employed in this issue, and the turbulence kinetic energy k ($m^2 \cdot s^{-2}$) and dissipation rate ε ($m^2 \cdot s^{-3}$) are determined by Eq (6) and (7), respectively.

$$\frac{\partial(\rho k)}{\partial t} + \frac{\partial(\rho k v_i)}{\partial x_i} = \frac{\partial}{\partial x_j}\left[\left(\mu + \frac{\mu_t}{\sigma_k}\right)\cdot\frac{\partial k}{\partial x_i}\right] + G_k + G_b - \rho\varepsilon - Y_M + S_k \quad (6)$$

$$\frac{\partial(\rho \varepsilon)}{\partial t} + \frac{\partial(\rho \varepsilon v_i)}{\partial x_i} = \frac{\partial}{\partial x_j}\left[\left(\mu + \frac{\mu_t}{\sigma_\varepsilon}\right)\cdot\frac{\partial \varepsilon}{\partial x_i}\right] + C_{1\varepsilon}\frac{\varepsilon}{k}(G_k + C_{3\varepsilon}G_b) - C_{2\varepsilon}\rho\frac{\varepsilon^2}{k} + S_\varepsilon \quad (7)$$

Where G_k and G_b are the turbulent kinetic energy generated by the average velocity and the turbulent kinetic energy generated by buoyancy, respectively, J; Y_M is the turbulent dissipation rate generated by compressible turbulence pulsation; S_k and S_ε are custom sources. The turbulent viscosity μ_t (Pa·s) was computed using k and ε as follows:

$$\mu_t = \rho C_\mu \frac{\varepsilon^2}{k} \quad (8)$$

where $C_{1\varepsilon}$, $C_{2\varepsilon}$, $C_{3\varepsilon}$, C_{μ}, σ_k, and σ_ε, are constants whose values, respectively, are 1.44, 1.92, 0.8, 0.09, 1.0, and 0.9, as suggested by Launder [24].

2.1.3 Computation Methodology

Based on the former reports [25], the numerical model shown in Figure 1 was built to investigate the influence of lance height and angle on the penetration depth in EAF steelmaking processes. In Figure 1, H_0 is the lance height, mm; H_s and h_g are, respectively, the depth of the molten steel and slag layer, mm; h_l is the penetration depth of molten steel, mm; D_0 is the hydraulic diameter of the molten bath, mm; D_e is the diameter of the jet exit, mm; θ is the angle of the jet injection, degrees. And it can be obtained that $H=(H_0-h_g)/sin\theta$ from Figure 1. Figures 2 and 3 show the geometric representation and the representative grids used in the simulations.

Three lance heights and three lance angles were studied in the numerical simulations to analyze the penetration depth of inclined coherent and conventional supersonic jets. And the parameters and physical properties of the fluids used in the numerical simulations were depicted in Tables 1 and 2.

The coherent supersonic jet nozzle adopted in this study was designed according to following conditions: 1) the design flow rates are 2500 Nm^3/h, for main oxygen and the Mach number is 2.0; 2) the working pressure is 101325 Pa; 3) the temperature of the oxygen source is 298 K. Figure 4 depicts the structure of the Laval nozzle, and its inlet, throat, and exit diameters are, respectively, 40.4 mm, 26.3 mm, and 34.2 mm.

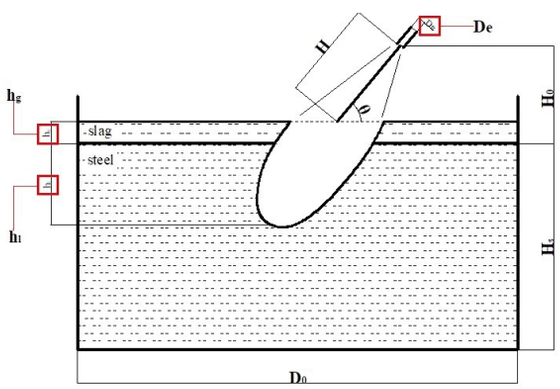

Figure 1. *Model of the inclined supersonic jet impinging cavity*

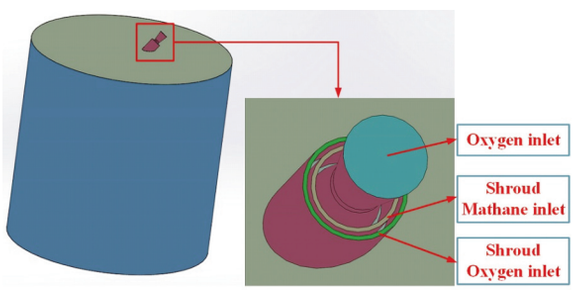

Figure 2. *Physical model of the inclined supersonic jet impinging cavity*

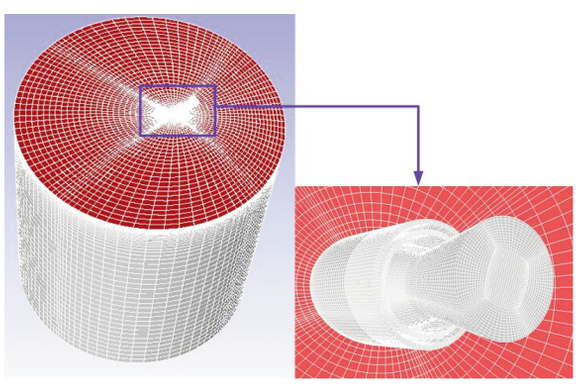

Figure 3. *Numerical model of the inclined supersonic jet impinging cavity*

A nonslip condition was applied to the walls whereas a standard wall function was adopted. Mass-flow inlet boundary conditions were adopted at the gas inlets. A pressure-out boundary condition was adopted for the outlet and the gauge pressure was 101325 Pa. The calculations were conducted in a transient solution mode and the pressure-velocity was coupled in PISO scheme. The pressure was set using the Body Force Weighted discretization scheme and Geometric reconstruction for the interface interpolation method. The momentum and mass equations were solved using second-order upwind schemes. The numerical simulations were observed to be convergent as the residuals of energy and other dependent variables were less than 10^{-6} and 10^{-3}, respectively.

2.2 Hydraulic Experiment and CFD Model Validation

As shown in Figure 5, a hydraulic experiment was conducted to investigate the influence of lance height and angle on the penetration depth of inclined supersonic jets and verify the CFD model built in Section 2.1. The hydraulic model was designed by a geometric ratio 1:4, and its parameters were listed in Table 1. In this experiment, water, oil, and air were used to present the molten steel, liquid slag, and oxygen, respectively. The lance height and lance angle can be adjusted by the regulator. A high-speed camera was used to capture the instantaneous motion and transient behavior of the jet impingement in the liquid bath at the speed of 20 fps. The penetration depth was measured at different lance heights and lance angles, as listed in Table 1. As methane combustion is very difficult and dangerous to model in a hydraulic experiment, we put a conventional supersonic jet as a substitute. The hydraulic model was simulated using the present CFD approach under the same conditions.

Figure 6 shows the transient impinging process at different lance heights at the lance angle θ=44° in the hydraulic experiment. Rows (a) and (b) show the

Table 1. *Parameters used in the present numerical simulations*

Items	CFD model	Hydraulic model
Molten bath hydraulic diameter, D_0 (mm)	2600	650
Molten steel depth, Hs (mm)	1200	300
Slag layer thickness, h_g (mm)	150	37
Lance height, H_0 (mm)	500,600,700	125,150,175
lance angle,θ(°)	40,42,44	44

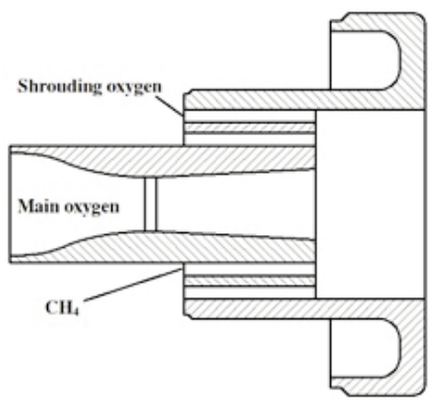

Figure 4. *Structure of the coherent supersonic jet*

Table 2. *Physical properties of the fluidscavity*

Items	Molten steel	Liquid slag	Oxygen	CH_4	Water	Oil
Density (kg·m^{-3})	7200	3000	1.29	0.68	997	925
Specific heat (J·kg^{-1}·K^{-1})	670	1200	919.31	2222	4182	-
Thermal conductivity (W·m^{-1}·K^{-1})	15	1.2	0.0246	0.0332	0.0242	0.6
Viscosity (kg·m^{-1}·s^{-1})	0.0065	0.35	1.92×10^{-5}	1.09×10^{-5}	7.98×10^{-3}	0.015
Surface tension (N·m^{-1})	1.6	0.4	--	--	0.071	0.029
Temperature (K)	1873	1873	298	298	298	298
	(1600ºC)	(1600ºC)	(25ºC)	(25ºC)	(25ºC)	(25ºC)

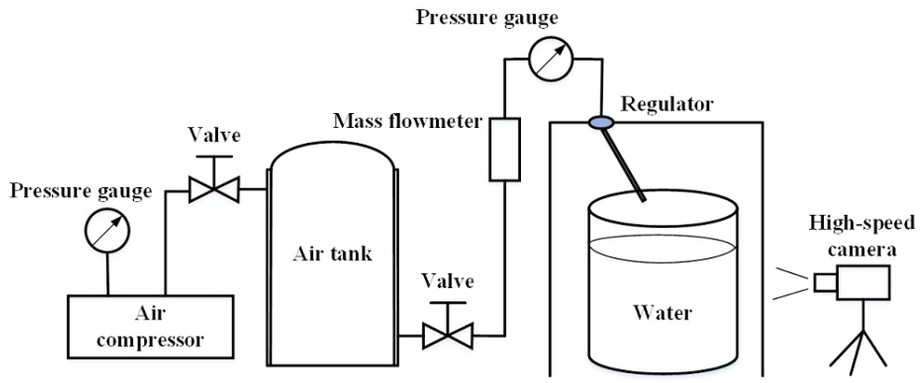

Figure 5. *Experimental set-up of the hydraulic experiment*

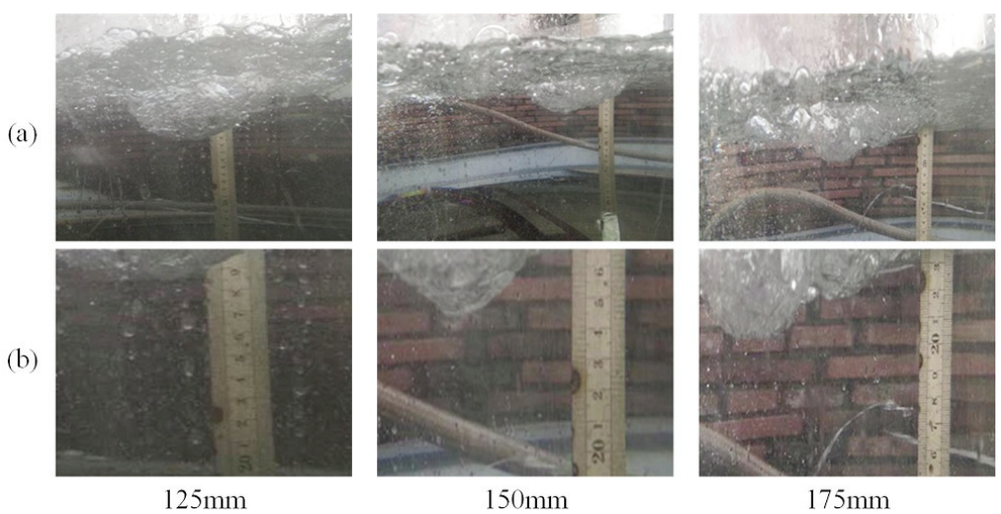

Figure 6. *Transient impinging process at different lance heights at the lance angle θ=44° in the hydraulic experiment; (a) the original pictures and (b) the corresponding enlarged pictures*

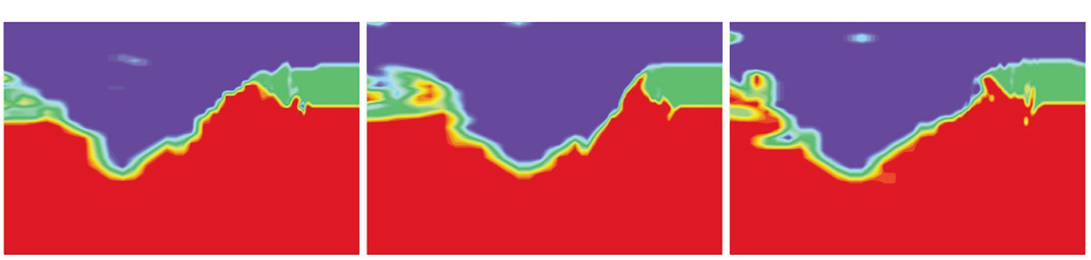

Figure 7. *Contours of the jet impact zone at different lance heights in the numerical simulations*

original and corresponding enlarged pictures, respectively. Figure 7 shows the contours of jet impact zone in numerical simulations of different lance heights based on hydraulic experiments. Figure 8 shows the penetration depth at the lance angle θ=44° in the hydraulic experiments and numerical simulations under different lance heights. It indicates that the numerical simulation results meet the hydraulic experiment results well with the maximum error being 5.34% and the average error being 4.69%. Hence, we can conclude that the results of the hydraulic experiment are consistent with the numerical simulation results.

3. Theoretical Model Optimized with Numerical Simulation

3.1 Assumptions

(1) The surface tension of the molten bath was ignored.

(2) The foaming of slag layer during the

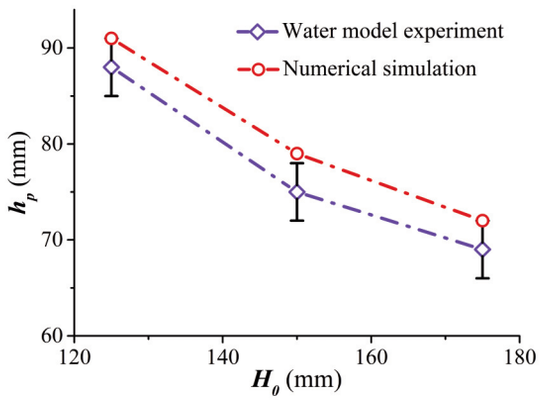

Figure 8. *Penetration depth at different lance heights at the lance angle θ=44° in the hydraulic experiment and numerical simulations*

steelmaking process was not considered.

(3) The oxygen jet was regarded as an ideal compressible gas.

(4) Oxygen was absorbed completely during the interaction between oxygen and the molten bath.

(5) The cross-section of the impact zone was regarded as a circle.

3.2 Theoretical Modeling of the Penetration Depth of the Inclined Jet

Based on the principle of energy conservation, the pressure of the jet centerline at the bottom of the impinging cavity P_l equals the static pressure of the molten bath, which is as expressed by Eq. (9):

$$P_l = \frac{1}{2}\rho_g v^2 = \rho_{steel} g h_l + \rho_{slag} g h_g \tag{9}$$

where ρ_g, ρ_{steel}, and ρ_{slag} are, respectively, the densities of the jet, steel, and slag, kg·m^{-3}; v is the jet centerline velocity at the bottom of the impinging cavity, m·s^{-1}.

According to Crowe's report [26], P_l and P_b can be obtained as follows:

$$P_l = \zeta Ar_b^{\frac{1}{2}} P_b \tag{10}$$

$$P_b = \frac{I_b}{A_b} \tag{11}$$

where ς is an empirical constant, ς=1.1–1.3. Ar_b is the Archimedes number of the jet at the molten bath surface; P_b is the pressure of the jet centerline at the molten bath surface.

Based on the momentum conservation of the jet impinging process, Eq. (12) can be obtained:

$$I_b = \rho_b v_b^2 A_b = \rho_e v_e^2 A_e = I_e \tag{12}$$

where I_b and I_e are the momenta at the molten bath and jet exit, respectively, kg·m·s^{-1}; v_b and v_e are the velocities at the molten bath and jet exit, respectively, m·s^{-1}; A_b and A_e are the jet areas at the molten bath and jet exit, respectively, m^2; ρ_b and ρ_e are the jet densities at the molten bath and jet exit, respectively, kg·m^{-3}.

Using the orthogonal decomposition, the momentum perpendicular to the molten bath direction can be obtained.

$$\rho_b v_b^2 A_b \sin\theta = \rho_e v_e^2 A_e \sin\theta \tag{13}$$

where θ is the horizontal angle of the lance. Further, the pressure of molten bath surface can be obtained as follows:

$$P_l = \sigma Ar_b^{\frac{1}{2}} P_b = \sigma Ar_b^{\frac{1}{2}} \frac{\rho_e v_e^2 A_e}{A_b} = \rho_{steel} g h_l + \rho_{slag} g h_g \tag{14}$$

Thus, the following equation can be obtained:

$$P_b = \frac{\rho_e v_e^2 A_e \sin\theta}{A_b} = \frac{\rho_e v_e^2 \sin\theta}{D_e}\left(\frac{\rho_b}{\rho_e}\right)\left(\frac{kD_e}{H}\right)^2 \tag{15}$$

where D_e and D_b are the diameters of the jet exit and diameter at the molten bath surface, respectively, and the relationship between these two factors can be expressed as follows:

$$D_b = \left(\frac{\rho_e}{\rho_b}\right)^{\frac{1}{2}}\left(\frac{v_e}{v_b}\right) D_e \tag{16}$$

In this study, a dimensionless value k was used, which is expressed as follows:

$$k = \left(\frac{v_b}{v_e}\right)\left(\frac{H}{D_e}\right) \tag{17}$$

By combining Eqs. (14) – (17), the following equation can be obtained:

$$h_l = \xi Ar_b^{\frac{1}{2}} \frac{\rho_e v_e^2}{\rho_{steel} g}\left(\frac{\rho_b}{\rho_e}\right)\left(\frac{kDe}{H}\right)^2 - \frac{\rho_{slag}}{\rho_{steel}} h_g \tag{18}$$

According to Melton's report [27], Ar_b, which indicates the ratio of the liquid buoyancy to the jet inertia force, can be obtained using the following equation:

$$Ar_b = \frac{\rho g D_b}{\rho_b v_b^2} = \frac{\rho g}{\rho_b v_b^2}\left(\frac{\rho_e}{\rho_b}\right)^{\frac{1}{2}}\left(\frac{H}{k}\right) \tag{19}$$

From Section 2.1.3, we know that H=(H_0-h_g)/sinθ. Finally, h_l can be obtained by combining Eq. (18) and Eq. (19).

$$h_l = \xi \frac{(\rho_e\rho_b)^{\frac{1}{4}} \rho^{\frac{1}{2}} v_e \sin^{\frac{3}{2}}\theta De}{\left(\rho_{steel}^2 g\right)^{\frac{1}{2}}}\left(\frac{k}{H_0 - h_g}\right)^{\frac{1}{2}} - \frac{\rho_{slag}}{\rho_{steel}} h_g \tag{20}$$

$$h_p = h_l + h_g = \xi \frac{(\rho_e\rho_b)^{\frac{1}{4}} \rho^{\frac{1}{2}} v_e \sin^{\frac{3}{2}}\theta De}{\left(\rho_{steel}^2 g\right)^{\frac{1}{2}}} \cdot \left(\frac{k}{H_0 - h_g}\right)^{\frac{1}{2}} + \frac{\rho_{steel} - \rho_{slag}}{\rho_{steel}} h_g \tag{21}$$

Thus, the theoretical model for calculating the inclined jet penetration depth h_p can be obtained. It can be observed that the dimensionless value k, lance height H_0, and lance angle θ are the key parameters for h_p calculation for a specific oxygen lance. It is necessary to obtain the exact k, v_e, ρ_b, and ρ_e values to improve the accuracy and validity of theoretical model.

The penetration depth of the inclined coherent and conventional supersonic jets is described by establishing an optimized theoretical model, which was used to calculate the jet penetration depth h_p by combining the theoretical model and numerical simulations. The main factors, i.e., k value, v_e, ρ_e, and ρ_b, can be calculated and exported by the CFD model and the UDF program to simulate the fluid flow characteristics of the inclined coherent and conventional supersonic jets and to process data in the procedure. It can be observed that these four main factors can be used in the theoretical model to calculate the jet penetration depth h_p. In Section 4.2, we show how the optimized theoretical model for h_p is modified to obtain a more accurate value.

4. Results and Discussions

4.1 k Value Analysis

In section 3.2, we have defined a newly dimensionless value k, which is one of the key factors to describe the jet impact characteristics. In Eq. (17), the dimensionless value v_b/v_e reflects the variation of jet velocity related to the jet exit velocity at the jet free distance (H/De), which is also non-dimensional. For a Laval nozzle, v_e and De are constants. Therefore, v_b and H are decisive factors for the calculation of the k value. Compared with the approach that uses v_b to analyze the jet impact characteristics as proposed by other researchers[4,5], these dimensionless numbers can improve the generalization ability of the mathematical formula in the modeling process.

Figure 9 shows the variation of k value of the inclined coherent and conventional supersonic jets. The k value increases and thereafter decreases after the Laval nozzle is exited in both cases. However, their specific variation tendencies are different. For the coherent supersonic jet, the k value is linearly correlated with the axial free distance from the nozzle at 0 m $\leq H \leq$ 1.5 m, and it thereafter decreases at H>1.5 m. However, the k value shows the same variation tendency in the region 0 m $\leq H \leq$ 0.5 m for the conventional supersonic jet, thereafter remains steady at 0.5 m $\leq H \leq$ 2.0 m, and finally declines when H>2.0 m. Comparing to the conventional supersonic jet, the k value of the coherent supersonic jet is bigger when $H \geq$ 0.5 m. As a result, H is the common dependent variable for the calculation of the k value in both cases. Hence, in the present studies, the k value is studied by analyzing the change in v_b.

Figure 10 shows the axial velocity distributions of the inclined coherent and conventional supersonic jets at the jet centerline. The axial velocity fluctuates recurrently after the Laval nozzle is exited in both cases because of incorrect expansion of jets. After recurrent fluctuations of the supersonic oxygen jet, the axial velocity of the jet reaches a steady state. The potential core length of the conventional supersonic jet is more than three times smaller than that of the coherent supersonic jet. The length of the coherent supersonic jet reaches 1.5 m, whereas that of the conventional supersonic jet is only 0.5 m. The shrouding flow injection and the concomitant combustion of methane account for the attenuation characteristics of the main supersonic oxygen jet.

4.2 Analysis of the Inclined Jet Penetration Depth

Figure 11 presents the penetration depth of the inclined coherent and conventional supersonic jets based on the numerical calculation at different lance heights and lance angles. As shown in Figure 11, the penetration depth decreases with the increase in the

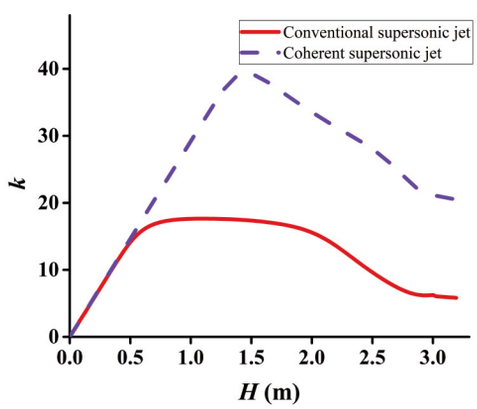

Figure 9. *Variation of k value of inclined coherent and conventional supersonic jets*

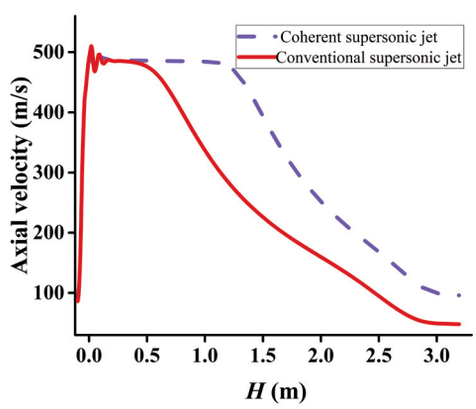

Figure 10. *Axial velocity distributions of inclined coherent and conventional supersonic jets*

lance height at the same lance angle; it also decreases with the decrease in the lance angle at the same lance height. Moreover, it can be observed that the penetration depth of the inclined coherent supersonic jet is larger than that of the inclined conventional supersonic jet at the same lance height and lance angle. This further indicates that, compared with the conventional supersonic jet, the coherent supersonic jet has a better stirring effect to the liquid bath. Moreover, the linear regression gradient of the inclined coherent supersonic jet is approximately 0.20 when the lance height H_0 is in the range 0.50–0.70 m at the same lance angle, whereas that of the inclined conventional supersonic jet is approximately 0.667. The main reason for this phenomenon is the difference of the potential core length between coherent supersonic jet and conventional supersonic jet, which was analyzed in Section 4.1. And it is evident from Figure 11 that the axial velocity attenuation of the coherent supersonic jet is slower than that of the conventional supersonic jet when the lance height and lance angle are in the ranges 0.5–0.7 m and 40–44°, respectively, which indicates that the axial distance is in the range 0.78–1.09 m.

Figures 12 and 13 show the contours of the impingent zone in the molten steel caused by the inclined coherent and conventional supersonic jets at different lance heights and angles. It is apparent that, compared with the inclined conventional supersonic jet, the inclined coherent supersonic jet has a deeper impact cavity at the same lance height and lance angle. As previously reported[8], three impingement modes (penetrating mode, splashing mode, and dimpling mode) are presented, which result from the jetting of a gas onto a liquid surface. As the lance height increases (or the lance angle decreases), the impingement mode goes from the penetration mode to the splashing mode, and end up with the dimpling mode.

4.3 Error analysis

In Section 3.2, the theoretical model for the prediction of penetration depth for the inclined coherent and conventional supersonic jets was established. The parameters k value, ρ_b, ρ_e, and v_e

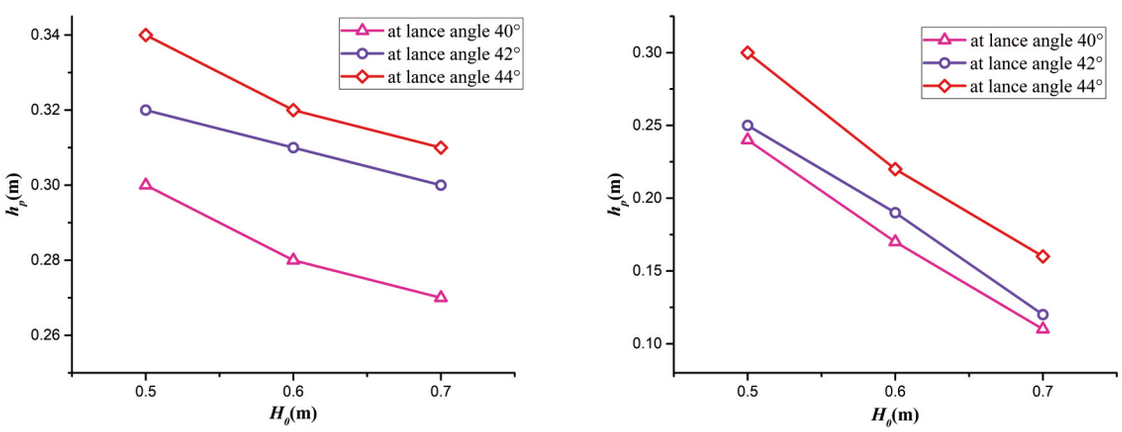

Figure 11. *CFD results of the penetration depth at different lance heights and angles for inclined (a) coherent supersonic jets and (b) conventional supersonic jets*

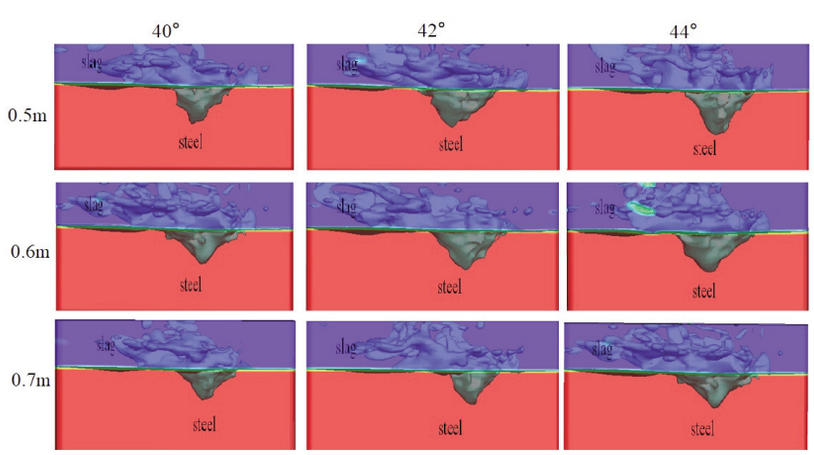

Figure 12. *Contours of the jet impinging caused by inclined coherent supersonic jet at different lance heights and angles*

Table 3. *Relevant parameters for the theoretical model of inclined coherent supersonic jet penetration depth*

Lance height H_0(m)	0.5			0.6			0.7		
Lance angle θ(°)	40	42	44	40	42	44	40	42	44
H(m)	0.54	0.52	0.5	0.7	0.67	0.65	0.86	0.82	0.79
ρ_e (kg/m^3)	2.3								
v_e (m/s)	489								
k	15.8	15.3	14.7	20.4	19.6	19	25.2	24	23.1
ρ_b(kg/m^3)	1.95	1.93	1.92	1.83	1.81	1.8	1.74	1.72	1.7

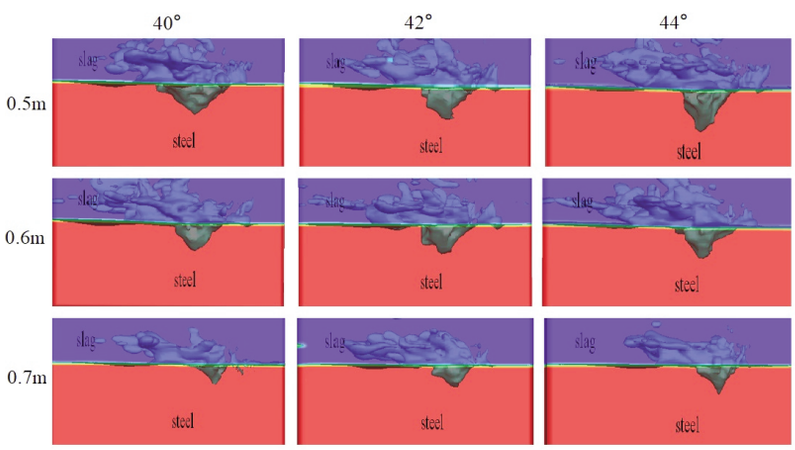

Figure 13. *Contours of the jet impinging caused by inclined conventional supersonic jet at different lance heights and angles*

Table 4. *Relevant parameters for the theoretical model of inclined conventional supersonic jet penetration depth*

Lance height H_0(m)	0.5			0.6			0.7		
Lance angle θ(°)	40	42	44	40	42	44	40	42	44
H(m)	0.54	0.52	0.5	0.7	0.67	0.65	0.86	0.82	0.79
ρ_e (kg/m^3)	2.3								
v_e (m/s)	489								
k	14.9	14.5	14.1	16.8	16.7	16.4	17.5	17.4	17.3
ρ_b(kg/m^3)	1.18	1.32	1.46	0.63	0.68	0.74	0.46	0.48	0.51

under different lance heights and lance angles were obtained from the results of the numerical simulations. Subsequently, these parameters were imported into the theoretical model to determine the values of h_p under different lance heights and lance angles. Tables 3 and 4 list the values of these parameters for inclined coherent and conventional supersonic jets at different lance heights and lance angles, respectively. It can be observed that the values of ρ_e and v_e are equal for these two kinds of supersonic jets as their central Laval nozzles share the same design dimensions.

Table 5 compares the values of h_p calculated using the theoretical model with those obtained from the numerical simulations. For the inclined coherent supersonic jet, the penetration depths obtained by using the theoretical model are very close to the CFD results. The maximum and minimum errors are 8.20% and 0.87%, respectively, except when the lance height H_0 is 0.7 m and the lance angle θ is 40°, in which case, the error reaches even 10.00%. Similar situations can be observed for the inclined conventional supersonic jet; the theoretical model results are consistent with the CFD results when (H_0, θ) is (0.50 m, 40°), (0.50 m, 44°), and (0.60 m, 44°). However, for other lance heights and angles, the results are significantly different, and the error is up to 22.58% when H_0 = 0.7 m and θ = 40°. Thus, when the lance height and lance angle are in certain ranges, it can be concluded that the theoretical model can accurately predict the

penetration depth of the inclined coherent and conventional supersonic jets, but it does not apply to situations in which the lance height and lance angle are out of the ranges.

The main factors that make the theoretical model results and the CFD results different are the uncertainties involved in the theoretical modeling. The Archimedes number Ar_b is influenced by not only the steel density ρ_{steel} but also the slag density ρ_{slag}. Nevertheless, we magnified Ar_b in this study because we only considered the steel density ρ_{steel}. As shown in Figures 6 and 7, a lower lance height at the same lance angle (or a larger lance angle at the same lance height) can form a deeper impact cavity for the inclined supersonic jets. Considering that the slag density is less than half of the steel density, it is important to consider the slag density in the calculation of Ar_b in these cases. Therefore, the results of the theoretical model are consistent with the CFD results. However, when a higher lance height and a smaller lance angle are set, which might lead to a shallow impact cavity where the penetration depth in the molten steel is even smaller than the thickness of the molten slag layer, the slag makes a slight impact on the buoyancy term of Ar_b. The accuracy of the theoretical model will be lower when we operate at higher lance heights and smaller lance angles, just because we ignored the effect of the molten slag in the theoretical modeling.

4.4 Optimized Modification of h_p Calculation

Based on the analysis of section 4.3, two optimized models for predicting the penetration depth of the coherent and conventional supersonic jets were obtained. The characteristic density ρ was used to calculate Ar_b during the theoretical and optimized models of the supersonic jets. Moreover, the optimized model, which combines theoretical model and two optimized models, is expressed for calculating h_p as follows. In optimized model 1, the characteristic density ρ is equal to half of the sum of ρ_{steel} and ρ_{slag}. In optimized model 2, ρ is equal to ρ_{slag}.

$$h_p = h_l + h_g = \xi \frac{(\rho_e \rho_b)^{\frac{1}{4}} \rho^{\frac{1}{2}} v_e \sin^{\frac{3}{2}} \theta De}{\left(\rho_{steel}^2 g\right)^{\frac{1}{2}}} \cdot \left(\frac{k}{H_0 - h_g}\right)^{\frac{1}{2}} + \frac{\rho_{steel} - \rho_{slag}}{\rho_{steel}} h_g$$

Optimized model:

$$\rho = \begin{cases} \rho_{steel} & \textit{Theoretical model} \\ \dfrac{\rho_{steel} + \rho_{slag}}{2} & \textit{Optimized model 1} \\ \rho_{slag} & \textit{Optimized model 2} \end{cases}$$

Figure 14 depicts the penetration depth of the inclined coherent supersonic jet at different lance heights and lance angles as obtained from the optimized model and the numerical simulations. The CFD results are consistent with the results of the optimized model. The penetration depth of the inclined coherent supersonic jet can be predicted accurately via the synthetical calculation of the optimized model. For the inclined coherent supersonic jets examined in this issue, the optimized model can be applied to the jet penetration depth calculation under the conditions 0.5 m$<H_0<$0.7 m and 40°$<\theta<$44°. Similarly, as shown in Figure 15, we can also predict the penetration depth of the inclined conventional supersonic jets accurately using the optimized model.

Tables 6 and 7 list the values of h_p of the inclined coherent and conventional supersonic jets calculated using the optimized model. Compared with the CFD results, the errors are less than 6.67% for the inclined coherent supersonic jet and 9.16% for the inclined conventional supersonic jet. Thus, the penetration depth can be accurately predicted using the optimized model.

As shown in Tables 6 and 7, there remain some differences between the CFD results and the results of the optimized model. The sources of the differences may be as follows:

(a) Interaction between the oxygen jet and the molten bath: In the theoretical modeling process, we

Table 5. *Values of h_p (penetration depth in the molten steel) at different lance heights and angles*

Lance height H_0 (m)		0.5			0.6			0.7		
Lance horizontal angle θ(°)		40	42	44	40	42	44	40	42	44
Coherent supersonic jet	CFD result	0.3	0.32	0.34	0.28	0.31	0.32	0.27	0.3	0.31
	Theoretical model	0.31	0.327	0.343	0.305	0.321	0.337	0.3	0.316	0.331
	Error(%)	3.23	2.14	0.87	8.2	3.43	5.04	**10**	5.06	6.34
Conventional supersonic jet	CFD result	0.24	0.25	0.3	0.17	0.19	0.22	0.11	0.12	0.16
	Theoretical model	0.251	0.279	0.307	0.193	0.216	0.237	0.152	0.169	0.185
	Error(%)	4.38	**10.39**	2.28	**13.26**	**12.04**	6.33	**22.58**	**17.16**	**13.52**

assumed that oxygen was absorbed completely during the interaction between oxygen and the molten bath, and we ignored the bounce-back effect of the oxygen jet in the impact cavity area. However, in the numerical simulations, all these conditions were taken into consideration. (b) Surface tension and the droplet generation of the molten bath: The influences of surface tension, droplet breakup, and splashing of the

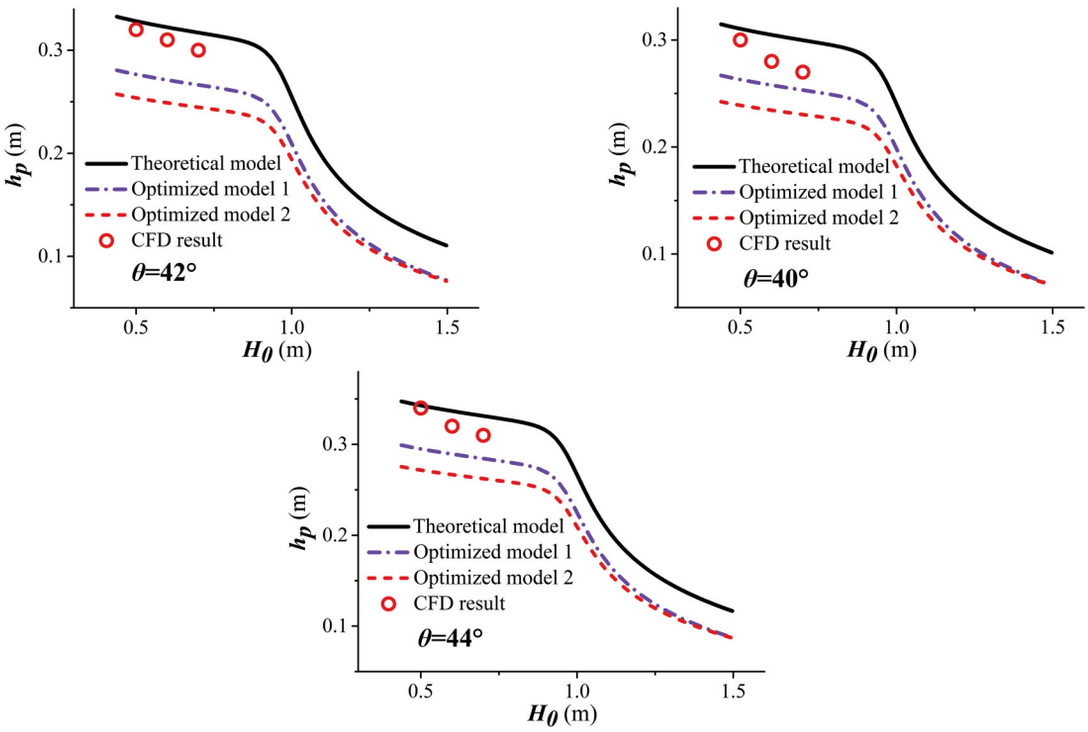

Figure 14. *Penetration depth of inclined coherent supersonic jet at different lance heights and lance angles*

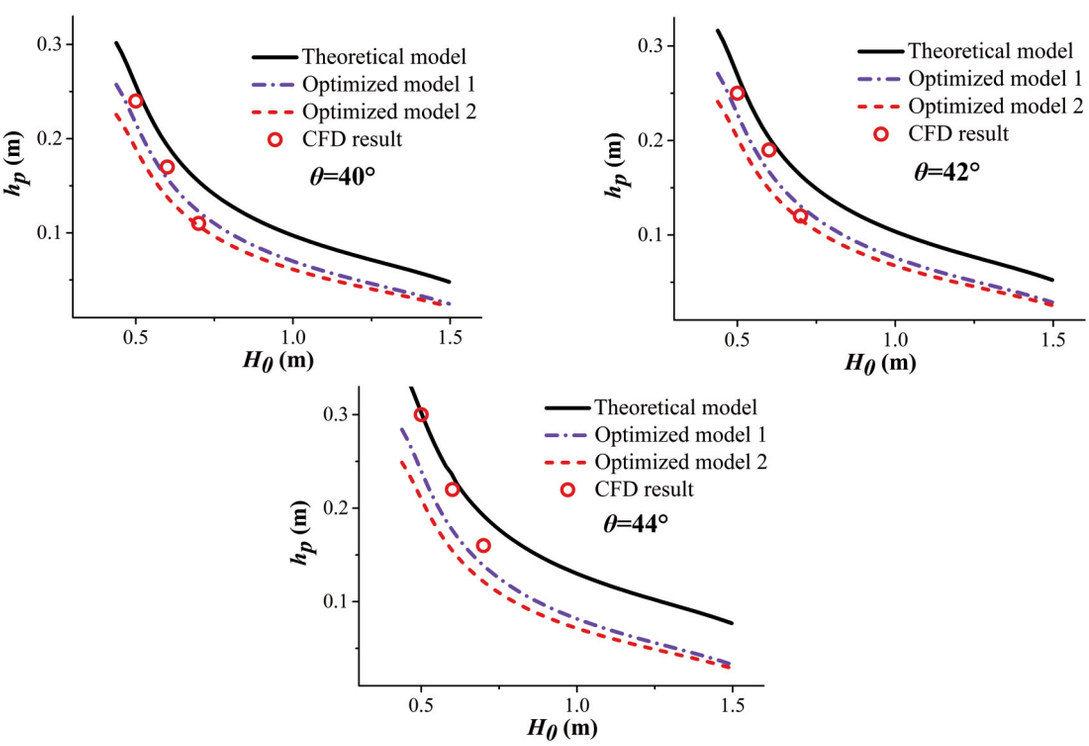

Figure 15. *Penetration depth of inclined conventional supersonic jet at different lance heights and lance angles*

Table 6. *Penetration depth of inclined coherent supersonic jet at different lance heights and lance angles*

Lance height H_0(m)	0.5			0.6			0.7		
Lance angle θ(°)	40	42	44	40	42	44	40	42	44
CFD result	0.3	0.32	0.34	0.28	0.31	0.32	0.27	0.3	0.31
Theoretical model	0.31	0.327	0.343		0.321	0.337		0.316	0.331
Optimized model 1				0.257			0.252		
Optimized model 2									
Error(%)	3.23	2.14	0.87	8.2	3.43	5.04	6.67	5.06	6.34

Table 7 *Values of h_p (m) at different lance heights and angles for inclined conventional supersonic jet*

Lance height H_0(m)	0.5			0.6			0.7		
Lance angle θ(°)	40	42	44	40	42	44	40	42	44
CFD result	0.24	0.25	0.3	0.17	0.19	0.22	0.11	0.12	0.16
Theoretical model	0.251		0.307			0.237			
Optimized model 1		0.235		0.165	0.182				0.156
Optimized model 2							0.1	0.109	
Error(%)	4.58	6	2.33	2.94	4.21	7.72	9.09	9.16	2.5

molten liquid on the jet impact characteristics were not considered in the optimized theoretical model. However, these factors play important roles in the calculation process of the CFD model.

5. Conclusions

In this paper, the influence of lance height and angle on the penetration depth of inclined coherent and conventional supersonic jets in EAF steelmaking processes was investigated using numerical simulations and hydraulic experiments. By combining theoretical modeling and numerical simulations, an optimized model was established to calculate the penetration depth of the inclined coherent and conventional supersonic jets. Finally, we come to the conclusions as follows:

(1) The applicability of numerical simulation model is verified through the results of numerical simulations and hydraulic experiments. By combining the CFD model and the theoretical model, the optimized model is brought out and it can accurately predict the penetration depth of the inclined coherent and conventional supersonic jets.

(2) Compared with the conventional supersonic jet, the potential core length is more than three times smaller than that of the coherent supersonic jet, which illustrates the change in the k value.

(3) The lance height and lance angle play an important role in the jet penetration depth. The penetration depth decreases with the increase in the lance height at the same lance angle, it also decreases with the decrease in the lance angle at the same lance height. Moreover, the penetration depth of the inclined coherent supersonic jet is larger than that of the inclined conventional supersonic jet for the same lance height and lance angle, which further indicates that, comparing with the conventional supersonic jet, the coherent supersonic jet has a better stirring effect to the liquid bath.

(4) The penetration depths of the inclined coherent and conventional supersonic jets can be accurately predicted using the optimized model combining the theoretical model and the CFD model. The error of the results between the numerical simulation and the theoretical model is no more than 8.21% for the inclined coherent supersonic jet and 9.16% for the inclined conventional supersonic jet.

Acknowledgements

Authors gratefully acknowledge the support by the National Nature Science Foundation of China (NSFC 51734003, 51604022 & 52004023).

References

[1] B. Lee, I. Sohn, JOM, 66 (2014) 1581-1594.

[2] G. Wei, R. Zhu, K. Dong, G. Ma,T. Cheng, Metall. Mater. Trans. B, 47 (2016) 3066-3079.

[3] G. Wei, R. Zhu, T. Cheng, F. Zhao, J. Iron Steel Inst., 23 (2016), 997-1006.

[4] M. Alam, J. Naser, G. Brooks, A Fontana, Metall. Mater. Trans. B, 41 (2010) 1354-1367.

[5] Q Li, M. Li, S. Kuang, Z. Zou, Metall. Mater. Trans. B, 46 (2015) 1494-1509.

[6] M. Li, Q. Li, S. Kuang,Z. Zou, Metall. Mater. Trans. B, 47 (2016) 116-126.

[7] R. D. Collins, H. Lubanska, J. Appl. Phys., 5 (2002) 22-26.

[8] N. A. Molloy, J. Iron Steel Inst., 226 (1970) 943-950.

[9] B. K. Rout, G. Brooks, Subagyo, M. Rhamdhani, Z. Li, Metall. Mater. Trans. B, 47 (2016) 3350-3361.

[10] J. Solórzano-López, R. Zenit, M. A. Ramírez-Argáez, Appl. Math. Model., 35 (2011) 4991-5005.

[11] A. Nordquist, N. Kumbhat, L. Jonsson, P. Jönsson, Steel Res. Int., 77 (2006) 82-90.

[12] M. Ersson, A. Tilliander, L. Jonsson, P. Jonsson, Trans. Iron Steel Inst. Jpn., 48 (2008) 377-384.

[13] D. Muñoz-Esparza, J. M. Buchlin, K. Myrillas, R. Berger, Appl. Math. Model., 36 (2012, 2687-2700.

[14] S. Sabah, G. Brooks, Metall. Mater. Trans. B, 47 (2016) 458-466.

[15] A. E. Wraith, R. Li, R. Harris, Chem. Eng. Sci., 30 (1995) 1057-1058.

[16] M. Alam, G. Irons, G. Brooks, A. Fontana, J. Naser, ISIJ Int., 51 (2011) 1439-1447.

[17] M. Alam, J. Naser, G. Brooks, Metall. Mater. Trans. B, 41 (2010) 636-645.

[18] M. Alam, J. Naser, G. Brooks, A. Fontana, ISIJ Int., 52 (2012) 1026-1035.

[19] I. Sumi, Y. Kishimoto, Y. Kikuchi, H. Igarashi, ISIJ Int., 46 (2006) 1312-1317.

[20] F. Liu, R. Zhu, K. Dong, S. Hu, Metall. Mater. Trans. B, 47 (2016) 1-16.

[21] G. Wei, R. Zhu, T. Cheng, K. Dong, L. Yang, X. Wu, Metall. Mater. Trans. B, 1 (2017) 361-374.

[22] G. Wei, R. Zhu, T. Cheng,K. Dong, R. Liu, Ironmaking Steelmaking, (2017) 1-11.

[23] Q. Li, M. Li, S. Kuang, Z. Zou, Can. Metall. Q., 53 (2014) 340-351.

[24] B.E. Launder, D.B. Spalding, Lect. Math. Model Turbul., Academic Press, London, (1972) 124-129.

[25] B. Bank, D.V. Chandrasekhara, J. Fluid Mech., 15 (1963) 13-33.

[26] C. T. Crowe, D. F. Elger, J. A. Roberson, Eng. Fluid Mech., John Wiley & Sons, Sharon, MA, USA, 2004.

[27] L. L. Melton, W. T. Malone, *J. Pet. Technol.*, 4 (1964) 56-66.

UTICAJ VISINE I UGLA KOPLJA NA DUBINU PENETRACIJE KOD NAGNUTE KOHERENTNE I KONVENCIONALNE NADZVUČNE MLAZNICE PRI PROIZVODNJI ČELIKA U ELEKTROLUČNOJ PEĆI

X.-T. Wu [a,b], R. Zhu [a,b], G.-S. Wei [a,b*], K. Dong [a,b]

[*a] Fakultet za metalurško i ekološko inženjerstvo, Univerzitet nauke i tehnologije u Pekingu, Peking, Kina

[b] Glavna laboratorija istraživačkog centra za posebno topljenje i pripremu vrhunskih metalnih materijala, Univerzitet nauke i tehnologije u Pekingu, Peking, Kina

Apstrakt

Danas su koherentne i konvencionalne nadzvučne mlaznice vrlo zastupljene u procesu proizvodnje čelika u elektrolučnim pećima. Uglavnom se ove mlaznice instaliraju u zid elektrolučne peći pod nagibom od 35–45°. Pa ipak, nema mnogo studija koje se bave uticajem koji imaju ove nadzvučne mlaznice postavljene pod nagibom. U ovom radu razvijen je optimiziran teoretski model za izračunavanje dubine penetracije koherentnih i konvencionalnih nadzvučnih mlaznica postavljenih pod nagibom kombinacijom teoretskog modeliranja i numeričke simulacije. Izvršena je validacija rezultata proračuna mehanike fluida na osnovu eksperimenata vodenog modela. Definisana je nova varijabla k da bi se iskazala varijacija brzine koja je u vezi sa izlazom mlaznice na slobodnoj udaljenosti. Rezultati optimiziranog teoretskog modela pokazuju da visina i ugao koplja utiču na dubinu penetracije nadzvučne mlaznice postavljene pod nagibom. Dubina penetracije se smanjuje ako nagib koplja ostaje isti a visina se povećava. Slično tome, dubina penetracije se smanjuje ako visina koplja ostaje ista, a smanjuje se nagib. Uz to, pod istim uslovima, dubina penetracije koherentne nadzvučne mlaznice postavljene pod nagibom je veća od dubine penetracije konvencionalne nadzvučne mlaznice postavljene pod nagibom. Optimizirani teoretski model može tačno da predvidi dubinu penetracije koherentnih i konvencionalnih nadzvučnih mlaznica.

Ključne reči: *Dubina penetracije; Mlaznice pod nagibom; Proizvodnja čelika u elektrolučnim pećima; Visina koplja; Nagib koplja*